Supplement of Biogeosciences, 22, 5413–5433, 2025
https://doi.org/10.5194/bg-22-5413-2025-supplement

Biogeosciences Open Access EGU

Supplement of

Temporal patterns of greenhouse gas emissions from two small thermokarst lakes in Nunavik, Canada

Amélie Pouliot et al.

Correspondence to: Amélie Pouliot (amelie.pouliot.1@ulaval.ca) and Daniel F. Nadeau (daniel.nadeau@gci.ulaval.ca)

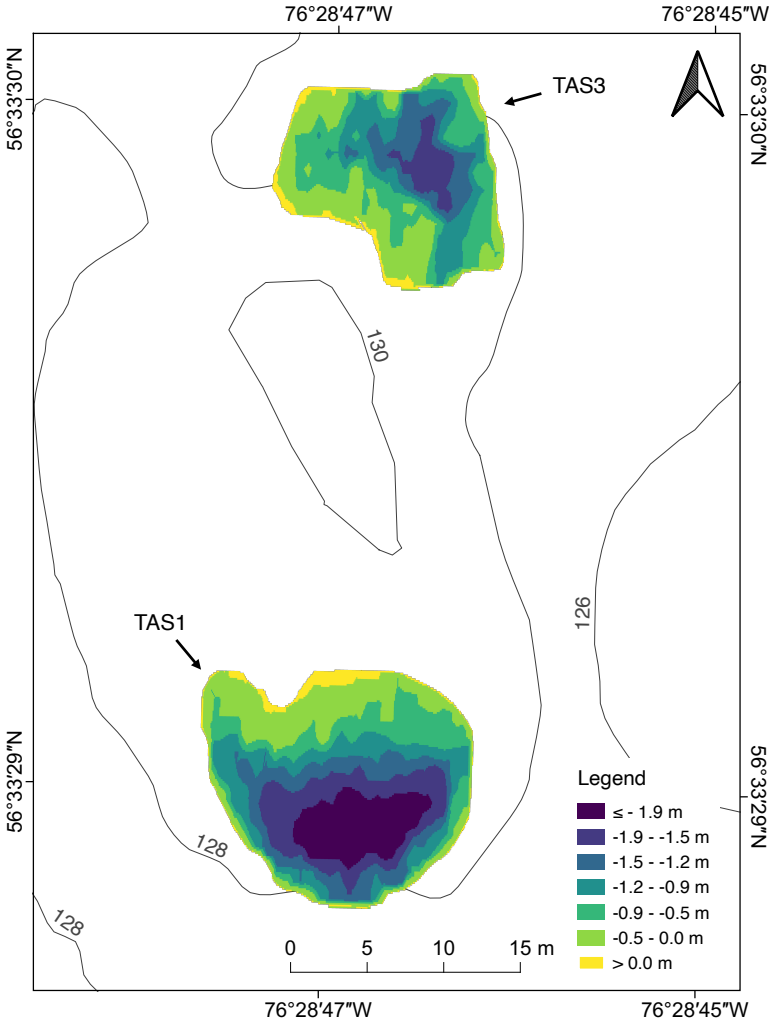

Figure S1. Bathymetric maps of lakes TAS1 and TAS3 obtained on 07 July 2022.

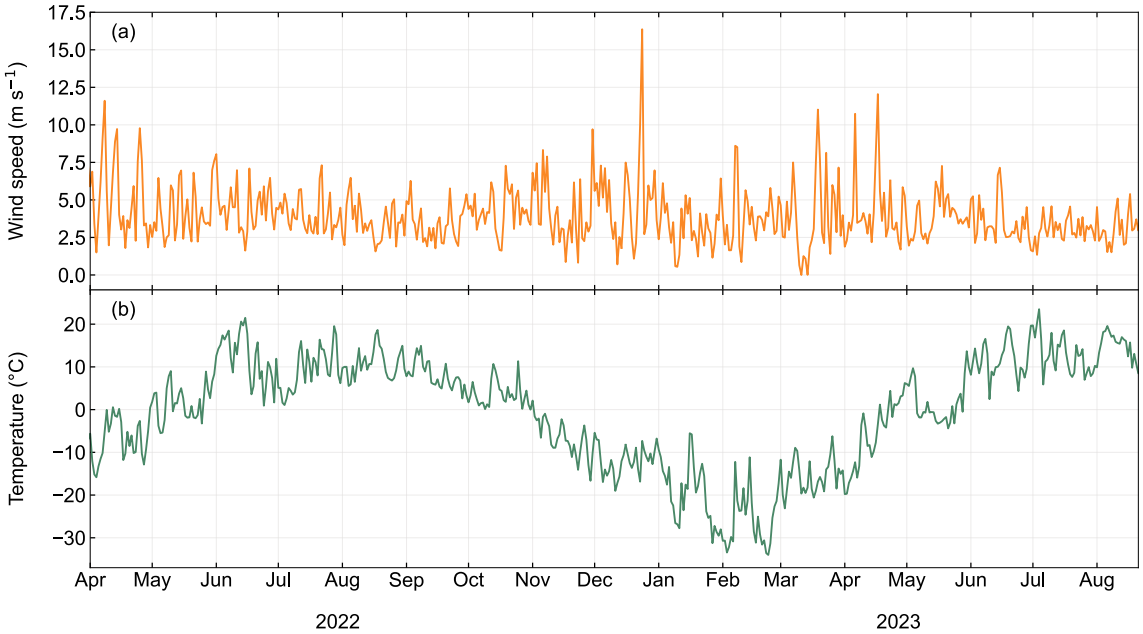

Figure S2. Weather conditions in the Tasiapik Valley from summer 2022 to summer 2023, showing (a) wind speed at 10 m and (b) air temperature. The brackets on top indicate the measurement campaign periods.

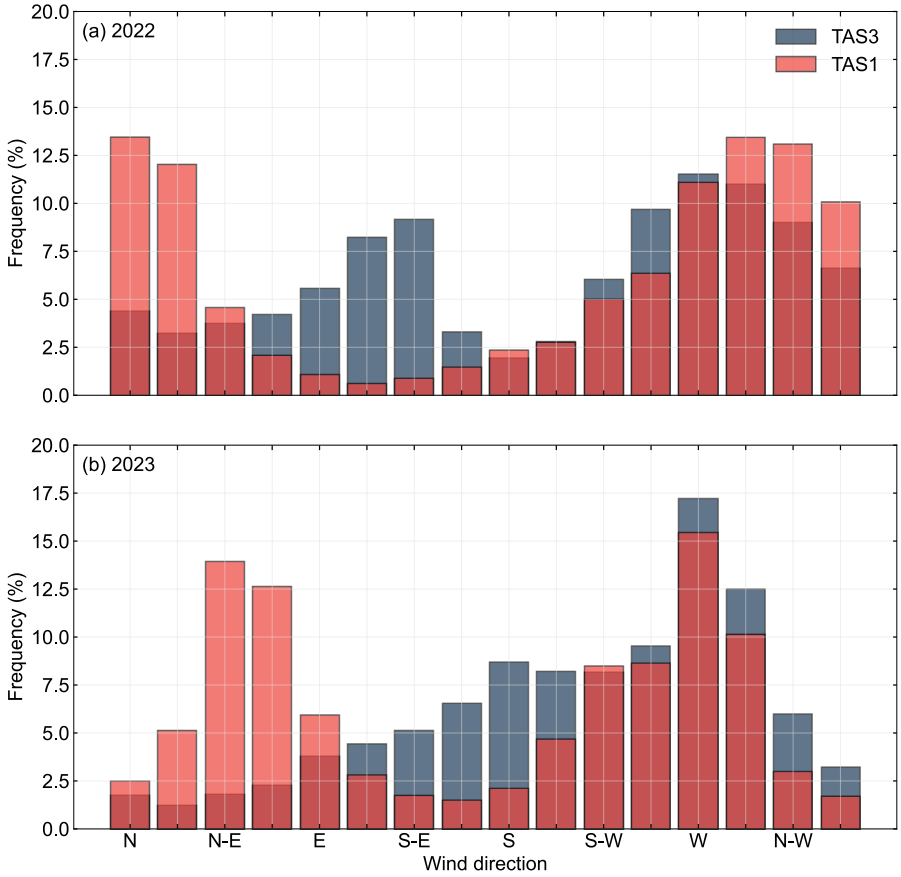

Figure S3. Wind direction frequency at lakes TAS1 and TAS3 for (a) July 2022 and (b) August 2023.

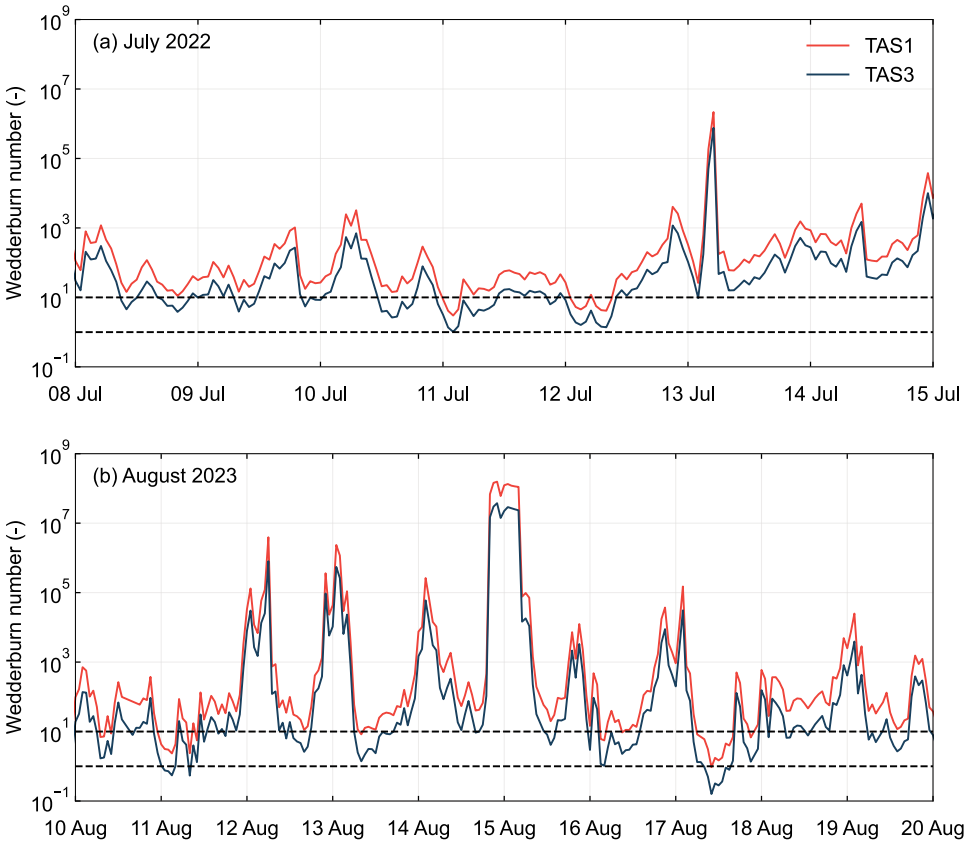

Figure S4. Wedderburn number (dimensionless) at lakes TAS1 and TAS3 during the measurement campaigns of (a) July 2022 and (b) August 2023.

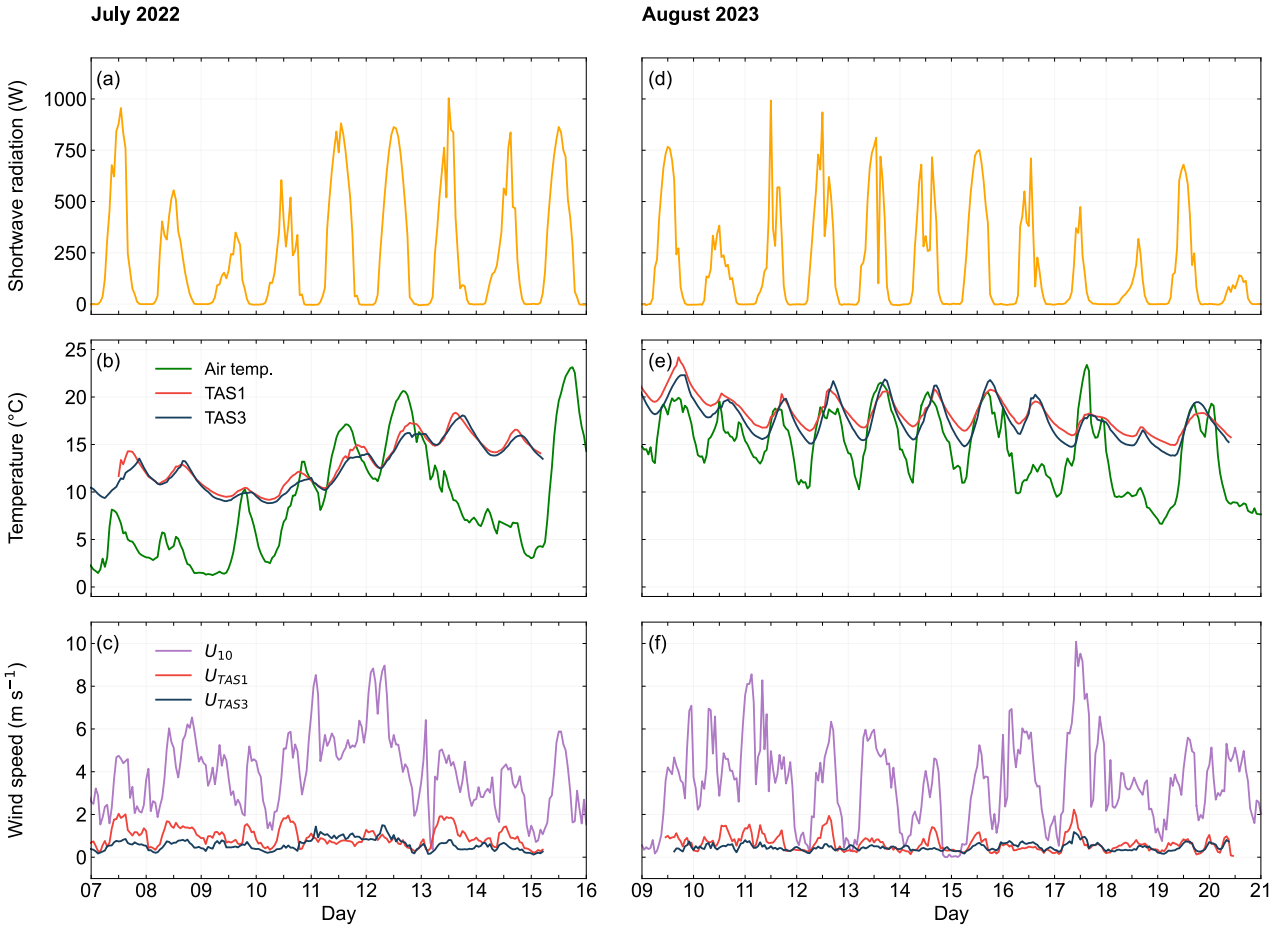

Figure S5. Shortwave radiation, air temperature, surface temperature in lakes TAS 1 and TAS3, and wind speed at 10 m in July 2022 (a, b, c) and August 2023 (d, e, f).

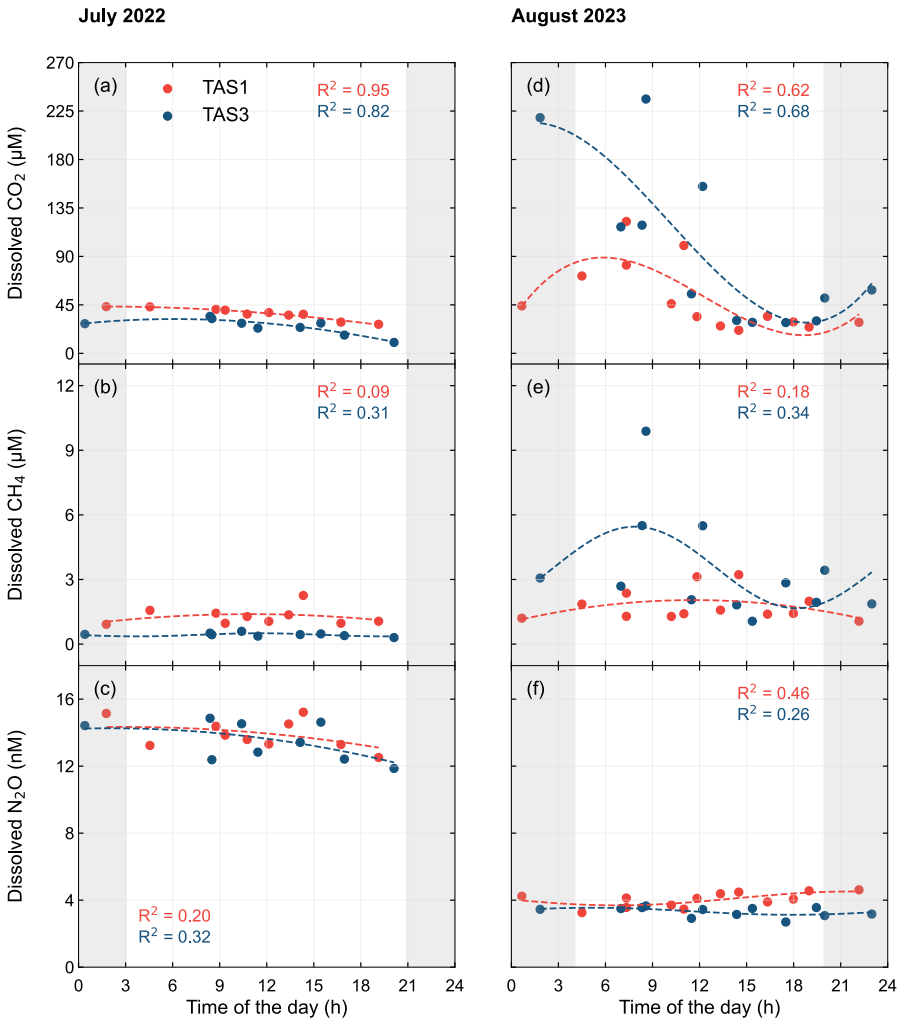

Figure S6. Diel cycles of near-surface concentrations of CO_2 (a,d), CH_4 (b,e) and N_2O (c,f) for the July 2022 (left) and August 2023 (right) intensive summer campaign periods for TAS1 and TAS3. The grey shaded areas indicate periods of zero solar radiation. Although the data are presented on a diurnal cycle, the measurements were taken over a two-week period (see Table S2). Coloured dotted lines represent sine-fitted trend lines. Time of day is expressed in EST.

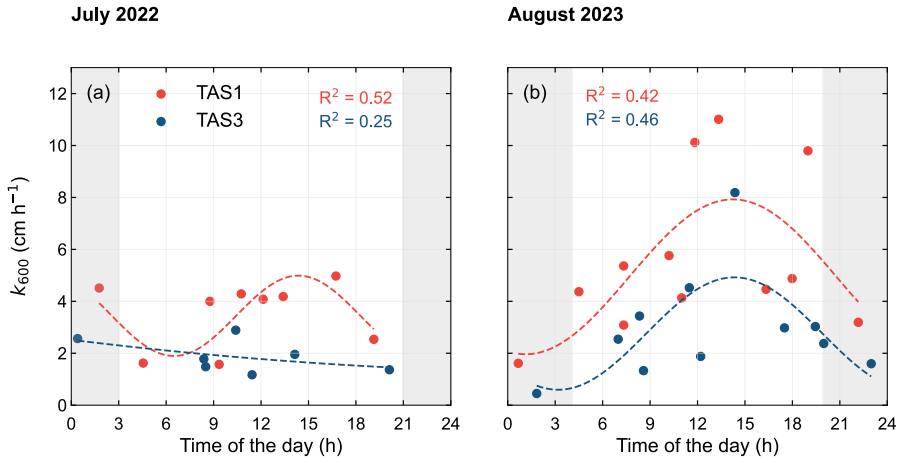

Figure S7. Diel cycles of gas transfer coefficient estimated from the gas chamber method in (a) July 2022 and (b) August 2023 for lakes TAS1 and TAS3. The grey shaded areas indicate periods of zero solar radiation. Although the data are presented on a diurnal cycle, the measurements were taken over a two-week period (see Table S2). Coloured dotted lines represent sine-fitted trend lines. Time of day is expressed in EST.

Table S1. Depth from lake bottom of the submersible automated data loggers of Temperature (HOBO U22-001), conductivity (HOBO U24-001, also measures temperature), pressure (HOBO U20L-01, also measures temperature), and dissolved oxygen (PME miniDOT, also measures temperature). Maximum depth varied between 248 and 290 cm in TAS1, and between 149 and 232 cm in TAS3.

Automated loggers	TAS1	TAS3
	Depth from bottom (cm)	
Pressure and temperature	18	22
Conductivity, oxygen and temperature	58	44
Temperature	97	66
Temperature	136	99
Temperature	176	121
Oxygen	193	144
Conductivity and temperature	210	144

Table S2. Chamber flux measurements at lakes TAS1 and TAS3 in July 2022 and August 2023. Time of day is expressed in EST.

	July 2022		August 2023	
Lake	Date	F_D CO_2 (mmol m^{-2} d^{-1})	Date	F_D CO_2 (mmol m^{-2} d^{-1})
TAS1	2022-07-07 9:14	14.40	2023-08-10 11:50	39.80
	2022-07-07 13:36	13.27	2023-08-11 19:10	15.51
	2022-07-11 01:59	16.81	2023-08-12 22:41	7.84
	2022-07-11 16:09	12.83	2023-08-13 18:18	14.45
	2022-07-12 11:53	17.06	2023-08-14 10:28	35.03
	2022-07-12 19:03	5.73	2023-08-14 13:48	22.26
	2022-07-13 08:37	6.89	2023-08-15 01:23	8.34
	2022-07-13 10:51	15.79	2023-08-15 16:55	19.79
	2022-07-15 04:19	6.53	2023-08-16 05:09	49.05
			2023-08-18 11:41	62.43
			2023-08-19 08:00	61.59
			2023-08-20 08:00	67.36
TAS3	2022-07-07 10:41	4.32	2023-08-10 13:44	44.82
	2022-07-07 14:22	2.51	2023-08-11 20:19	17.75
	2022-07-08 08:42	4.06	2023-08-12 23:36	13.50
	2022-07-11 00:59	2.72	2023-08-13 19:42	9.03
	2022-07-11 17:15	-1.44	2023-08-14 11:45	40.28
	2022-07-12 11:11	1.40	2023-08-14 14:42	27.25
	2022-07-12 19:47	-1.96	2023-08-15 02:15	16.84
	2022-07-13 09:50	4.07	2023-08-15 17:53	9.73
	2022-07-15 04:57	3.96	2023-08-16 07:18	49.14
			2023-08-18 12:46	51.02
			2023-08-19 08:54	50.61
			2023-08-20 09:03	66.35

Table S3. Diffusive fluxes of CO_2, CH_4, and N_2O in TAS1 and TAS3 (N = 9 in 2022; N = 12 in 2023) and ebullitive fluxes of CH_4 in 2023 (N = 4 for TAS1; N = 8 for TAS3). Values are expressed as mean ± standard deviation (min - max). na = not available.

	Lake	July 2022	August 2023
F_D CO_2 (mmol m^{-2} d^{-1})	TAS1	12.1 ± 4.6 (5.7 - 17.1)	33.6 ± 22.1 (7.8 - 67.4)
	TAS3	2.2 ± 2.4 (–2.0 - 4.3)	33.0 ± 19.6 (9.0 - 66.4)
F_D CH_4 (mmol m^{-2} d^{-1})	TAS1	0.8 ± 0.3 (0.3 - 1.1)	2.2 ± 1.9 (0.4 - 7.2)
	TAS3	0.2 ± 0.1 (0.1 - 0.3)	1.9 ± 1.1 (0.3 - 3.7)
F_D N_2O (µmol m^{-2} d^{-1})	TAS1	1.9 ± 1.0 (0.3 - 3.6)	–7.5 ± 3.5 (–13.2 - –2.1)
	TAS3	0.8 ± 0.4 (0.4 - 1.4)	–4.5 ± 3.0 (–12.1- –0.7)
F_E CH_4 (mmol m^{-2} d^{-1})	TAS1	na	1.9 ± 1.5 (0.5 - 3.9)
	TAS3	na	11.9 ± 4.5 (6.9 - 18.1)

Table S4. Dissolved gases measurements at lakes TAS1 and TAS3 in July 2022 and August 2023. Time of day is expressed in EST.

	July 2022				August 2023			
Lake	Date	CO_2 (µM)	CH_4 (µM)	N_2O (µM)	Date	CO_2 (µM)	CH_4 (µM)	N_2O (µM)
TAS1	2022-07-06 14:20	36.30	2.26	0.015	2023-08-09 14:30	21.43	3.22	0.004
	2022-07-07 08:46	40.90	1.44	0.014	2023-08-10 11:50	34.07	3.13	0.004
	2022-07-07 13:24	35.48	1.36	0.015	2023-08-11 18:59	24.39	1.99	0.005
	2022-07-11 01:46	43.34	0.92	0.015	2023-08-12 22:10	28.80	1.07	0.005
	2022-07-11 16:44	29.01	0.97	0.013	2023-08-13 17:59	29.19	1.42	0.004
	2022-07-12 12:08	37.85	1.06	0.013	2023-08-14 10:12	46.01	1.28	0.004
	2022-07-12 19:08	26.96	1.06	0.013	2023-08-14 13:20	25.41	1.58	0.004
	2022-07-13 09:21	40.12	0.97	0.014	2023-08-15 00:40	44.05	1.20	0.004
	2022-07-13 10:45	36.48	1.28	0.014	2023-08-15 16:20	34.32	1.39	0.004
	2022-07-15 04:33	43.20	1.57	0.013	2023-08-16 04:30	71.83	1.86	0.003
					2023-08-18 11:00	100.14	1.41	0.003
					2023-08-19 07:20	122.48	2.37	0.004
					2023-08-20 07:20	81.95	1.29	0.004
TAS3	2022-07-06 15:27	28.10	0.47	0.015	2023-08-09 15:22	28.79	1.06	0.004
	2022-07-07 10:24	27.95	0.59	0.015	2023-08-11 19:59	51.36	3.43	0.003
	2022-07-07 14:08	24.08	0.44	0.013	2023-08-12 22:59	58.84	1.87	0.003
	2022-07-08 08:23	34.33	0.51	0.015	2023-08-13 19:27	30.13	1.94	0.004
	2022-07-11 00:24	27.53	0.45	0.014	2023-08-14 11:29	55.25	2.06	0.003
	2022-07-11 16:57	16.97	0.39	0.012	2023-08-14 14:22	30.57	1.82	0.003
	2022-07-12 11:26	23.41	0.37	0.013	2023-08-15 01:50	218.85	3.07	0.003
	2022-07-12 20:07	10.15	0.30	0.012	2023-08-15 17:30	28.54	2.84	0.003
	2022-07-13 08:30	32.28	0.43	0.012	2023-08-16 06:59	117.43	2.69	0.003
					2023-08-18 12:12	154.99	5.49	0.003
					2023-08-19 08:35	236.16	9.88	0.004
					2023-08-20 08:20	119.01	5.50	0.004

Table S5. Bottom concentrations of CO_2, CH_4 and N_2O measured in lakes TAS1 and TAS3 with the headspace method. Values are expressed as mean ± standard deviation (min - max). N = 4 in 2022 and N = 2 in 2023. Water was sampled about 15 cm above sediments.

	July 2022		August 2023	
Bottom concentration	TAS1	TAS3	TAS1	TAS3
CO_2 (µM)	315.6 ± 225.6 (89.8 - 510.5)	333.4 ± 239.0 (135.1 - 646.8)	813.5 ± 3.4 (811.1 - 815.9)	770.4 ± 63.2 (725.7 - 815.1)
CH_4 (µM)	103.1 ± 81.1 (26.2 - 174.5)	92.3 ± 98.1 (16.3 - 222.7)	591.6 ± 97.9 (522.4 - 660.9)	400.1 ± 147.0 (296.2 - 504.0)
N_2O (nM)	11.3 ± 2.9 (7.3 - 14.0)	10.7 ± 3.3 (7.6 - 14.2)	-	-

Table S6. Gas transfer velocities (k_{600}) measured with the floating chamber in lakes TAS1 and TAS3 using surface GHG concentrations obtained by the headspace method. Time of day is expressed in EST.

	July 2022		August 2023	
Lake	Date	k_{600} (cm h^{-1})	Date	k_{600} (cm h^{-1})
TAS1	2022-07-07 09:14	4.00	2023-08-10 11:50	10.12
	2022-07-07 13:36	4.18	2023-08-11 19:10	9.80
	2022-07-11 01:59	4.51	2023-08-12 22:41	3.19
	2022-07-11 16:09	4.97	2023-08-13 18:18	4.88
	2022-07-12 11:53	4.08	2023-08-14 10:28	5.76
	2022-07-12 19:03	2.54	2023-08-14 13:48	11.01
	2022-07-13 08:37	1.57	2023-08-15 01:23	1.61
	2022-07-13 10:51	4.29	2023-08-15 16:55	4.46
	2022-07-15 04:19	1.62	2023-08-16 05:09	4.37
			2023-08-18 11:41	4.13
			2023-08-19 08:00	3.09
			2023-08-20 08:00	5.36
TAS3	2022-07-07 10:41	2.89	2023-08-11 20:19	2.38
	2022-07-07 14:22	1.96	2023-08-12 23:36	1.60
	2022-07-08 08:42	1.78	2023-08-13 19:42	3.03
	2022-07-11 00:59	2.57	2023-08-14 11:45	4.52
	2022-07-12 11:11	1.17	2023-08-14 14:42	8.19
	2022-07-12 19:47	1.36	2023-08-15 02:15	0.45
	2022-07-13 09:50	1.48	2023-08-15 17:53	2.98
			2023-08-16 07:18	2.54
			2023-08-18 12:46	1.88
			2023-08-19 08:54	1.33
			2023-08-20 09:03	3.43

Larger-scale estimates

To estimate annual GHG diffusive emissions from the lakes, we calculated the average, minimum, and maximum fluxes for summer 2022, fall 2022, spring 2023, and summer 2023 (see Table S6). For each season, Equation 4 was applied using the minimum and maximum concentration gradients estimated for that season (see Table S7), along with the average gas transfer velocity (k) (see Table S8) over the corresponding period. We estimated k_{600}, the gas transfer velocity normalized to a Schmidt number of 600, to calculate k with equation 5. Limnological seasons were defined based on changes in the thermal structure of the water column. For summer comparisons, the period from 7 July to 20 August was used, as data were available for both 2022 and 2023. Fall 2022 and spring 2023 were defined as the periods from September to October and mid-May to mid-June, respectively.

To estimate the concentration gradients for each season, different approaches were applied based on data availability. For the two summers, we used the average surface concentration measured during the two-week intensive campaigns. For fall 2022, in the absence of direct measurements, we estimated the summer storage flux from the dissolved gas concentration profiles recorded during the intensive campaigns. Given the lakes are very small, it was assumed that the GHG accumulating in deeper layers would have sufficient time to mix with surface waters and equilibrate with the atmosphere before ice cover formation. Thus, the theoretical surface concentration was calculated by mixing the water column gas concentrations, using the volume of each water layer derived from hypsographic curves, as described in Prėskienis et al. (2021). For spring 2023, we estimated surface concentrations using the ratio between summer and winter gas concentrations observed by Matveev et al. (2019), as no measurements under the ice were available to calculate the winter storage flux. Matveev et al. (2019) studied CH_4 and CO_2 concentrations beneath the ice of five thermokarst lakes in late winter and compared them with summer concentrations. These lakes are similar to those in this study, located in the subarctic region of Quebec, in peatland valleys near the Sasapimakwananisikw River. The lakes are shallow (maximum depth of 1.4 to 2.8 m) and contain high concentrations of organic matter, resulting in limited water transparency. The median ratios of dissolved gas accumulated in the water column (in mmol m^{-2}) for winter relative to summer were 0.67 for CO_2 and 1.06 for CH_4. These ratios were used to estimate storage concentrations, assuming that all GHGs accumulated under the ice would mix with surface waters and equilibrate with the atmosphere during spring before summer stratification. This assumption may not fully reflect reality, as Matveev et al. (2019) observed a very short mixing period in spring, with stratification quickly establishing after the ice cover disappeared, leaving only the upper part of the water column to release its gas content. Nevertheless, we considered this as a *potential* spring storage flux.

The average seasonal gas transfer coefficient k_{600} (cm h^{-1}), was calculated using the small eddy version of the surface renewal model (SRM) (Macintyre et al., 1995), which accounts for both heat exchange processes and wind-induced turbulence at the air-water interface:

$$k_{600} = c_1(\varepsilon\upsilon)^{\frac{1}{4}} S_c^{-\frac{1}{2}} \quad \text{(S1)}$$

where υ is the kinematic viscosity (m^2 s^{-1}), c_1 is an empirically derived coefficient, ε is the dissipation rate of turbulent kinetic energy (m^2 s^{-3}), and S_c is the Schmidt number defined above. The dissipation rates driven by wind shear (u_{*w}) and buoyancy flux under cooling (β) were computed following Tedford et al. (2014). Surface energy fluxes were derived from meteorological data and surface water temperatures recorded by automated thermistors installed in the lakes. The depth of the surface layer (i.e., the mixing epilimnion) was determined based on the rapid decline in dissolved oxygen (Fig. 5), which varied between years. In the summers 2022 and 2023, the surface layer depths were estimated at 2.1 m and 1.0 m for TAS1, and 1.1 m and 0.5 m for TAS3, respectively. During fall 2022 and spring 2023, the surface layer was assumed to extend to the bottom of the lakes. As noted in previous studies, uncertainty in the parameter c_1 limits the application of the SRM for estimating gas fluxes (Read et al., 2012; Zappa et al., 2007; Macintyre et al., 2010; Vachon et al., 2020; Macintyre et al., 2021). Theoretical and experimental studies suggest that c_1 typically approximates 0.4 (Zappa et al., 2007; Lamont and Scott, 1970), but can range between 0.2 and 1.0 depending on turbulence intensity, water depth, and surface cleanliness (Macintyre et al., 2018; Wang et al., 2015). Given that our lakes are smaller and shallower than those in previous studies, we adopted the lower boundary value of $c_1 = 0.2$.

Table S7. Seasonal diffusive flux estimates at lakes TAS1 and TAS3 across limnological seasons. For summer comparisons, the period from 7 July to 20 August was used; fall 2022 and spring 2023 correspond to September-October and mid-May to mid-June, respectively. Values are expressed as min - max for each period. na=not available.

Lake	F_D CO_2 (mmol m^{-2} d^{-1})	F_D CH_4 (mmol CO_2 eq. m^{-2} d^{-1})	F_D N_2O (mmol CO_2 eq. m^{-2} d^{-1})	GHG (mmol CO_2 eq. m^{-2} d^{-1})
Summer 2022				
TAS1	15.7 (4.7 - 34.4)	11.5 (3.4 - 24.9)	0.6 (0.2 - 1.3)	27.8 (8.2 - 60.6)
TAS3	5.8 (1.5 - 12.7)	4.4 (1.1 - 9.7)	0.5 (0.1 - 1.2)	10.7 (2.8 - 23.6)
Fall 2022				
TAS1	31.8 (3.4 - 79.3)	87.1 (9.3 - 216.5)	–0.3 (–0.0 - –0.8)	118.6 (12.7 - 295.1)
TAS3	59.1 (5.8 - 149.5)	171.5 (16.7 - 432.7)	–0.6 (–0.1 - –1.6)	230.0 (22.4 - 580.6)
Spring 2023				
TAS1	9.8 (1.8 - 18.5)	116.2 (21.4 - 218.3)	na	126.0 (23.2 - 236.8)
TAS3	31.0 (5.7 - 62.5)	212.1 (39.3 - 426.4)	na	243.1 (45.0 - 488.9)
Summer 2023				
TAS1	27.7 (4.0 - 63.2)	14.9 (2.2 - 34.0)	–1.5 (–0.2 - –3.5)	41.1 (6.0 - 93.7)
TAS3	80.2 (9.0 - 182.3)	36.8 (4.2 - 83.6)	–2.2 (–0.3 - –5.0)	114.7 (12.9 - 260.8)

Table S8. Average bottom concentrations of CO_2, CH_4, and N_2O in lakes TAS1 and TAS3 estimated across limnological seasons. These estimates were derived from summer average surface concentrations measured during the campaigns (for summer estimates), total gas concentrations in the water column during summer (for fall estimates), and the summer-to-winter gas concentration ratio reported by Matveev et al. (2019) (for spring estimates).

Lake	CO_2 (µM)	CH_4 (µM)	N_2O (nM)
Summer 2022			
TAS1	37.9	1.3	13.9
TAS3	25.0	0.4	13.5
Fall 2022			
TAS1	52.1	7.7	14.0
TAS3	70.0	13.3	13.5
Spring 2023			
TAS1	34.9	8.2	-
TAS3	46.9	14.1	-
Summer 2023			
TAS1	51.1	1.8	4.0
TAS3	94.2	3.5	3.3
Fall 2023			
TAS1	186.2	62.8	-
TAS3	275.9	99.8	-
Spring 2024			
TAS1	124.7	66.7	-
TAS3	184.8	106.0	-

Table S9. Gas transfer velocities (k_{600}) estimated with the surfacer renewal model in lakes TAS1 and TAS3 across limnological seasons. For summer comparisons, the period from 7 July to 20 August was used; fall 2022 and spring 2023 correspond to September-October and mid-May to mid-June, respectively. Values are expressed as mean (min-max).

Lake	k_{600} (cm h^{-1})
Summer 2022	
TAS1	3.0 (0.8 - 6.4)
TAS3	3.6 (0.9 - 7.9)
Fall 2022	
TAS1	3.0 (0.3 - 7.2)
TAS3	3.4 (0.3 - 8.1)
Spring 2023	
TAS1	3.3 (0.7 - 6.2)
TAS3	3.7 (0.8 - 6.9)
Summer 2023	
TAS1	3.0 (0.4 - 7.0)
TAS3	3.7 (0.4 - 8.8)

References

Lamont, J. C. and Scott, D. S.: An eddy cell model of mass transfer into the surface of a turbulent liquid, AICHE J., 16, 513-519, 10.1002/aic.690160403, 1970.

MacIntyre, S., Wanninkhof, R., and Chanton, J. P.: Trace gas exchange across the air-sea interface in fresh water and coastal marine environments, Biogenic Trace Gases : Measuring Emissions From Soil and Water, 52-97, 1995.

MacIntyre, S., Crowe, A. T., Cortés, A., and Arneborg, L.: Turbulence in a small arctic pond, Limnol. Oceanogr., 63, 2337-2358, 10.1002/lno.10941, 2018.

MacIntyre, S., Jonsson, A., Jansson, M., Aberg, J., Turney, D. E., and Miller, S. D.: Buoyancy flux, turbulence, and the gas transfer coefficient in a stratified lake, Geophys. Res. Lett., 37, L24604, 10.1029/2010GL044164, 2010.

MacIntyre, S., Bastviken, D., Arneborg, L., Crowe, A. T., Karlsson, J., Andersson, A., Gålfalk, M., Rutgersson, A., Podgrajsek, E., and Melack, J. M.: Turbulence in a small boreal lake: Consequences for air–water gas exchange, Limnol. Oceanogr., 66, 827-854, 10.1002/lno.11645, 2021.

Matveev, A., Laurion, I., and Vincent, W. F.: Winter Accumulation of Methane and its Variable Timing of Release from Thermokarst Lakes in Subarctic Peatlands, J. Geophys. Res.-Biogeosciences, 124, 3521-3535, 10.1029/2019JG005078, 2019.

Prėskienis, V., Laurion, I., Bouchard, F., Douglas, P. M. J., Billett, M. F., Fortier, D., and Xu, X.: Seasonal patterns in greenhouse gas emissions from lakes and ponds in a High Arctic polygonal landscape, Limnol. Oceanogr., 66, S117-S141, 10.1002/lno.11660, 2021.

Read, J. S., Hamilton, D. P., Desai, A. R., Rose, K. C., MacIntyre, S., Lenters, J. D., Smyth, R. L., Hanson, P. C., Cole, J. J., Staehr, P. A., Rusak, J. A., Pierson, D. C., Brookes, J. D., Laas, A., and Wu, C. H.: Lake-size dependency of wind shear and convection as controls on gas exchange, Geophys. Res. Lett., 39, L09405, 10.1029/2012GL051886, 2012.

Tedford, E. W., MacIntyre, S., Miller, S. D., and Czikowsky, M. J.: Similarity scaling of turbulence in a temperate lake during fall cooling, J. Geophys. Res.-Oceans, 119, 4689-4713, 10.1002/2014JC010135, 2014.

Vachon, D., Langenegger, T., Donis, D., Beaubien, S. E., and McGinnis, D. F.: Methane emission offsets carbon dioxide uptake in a small productive lake, Limnol. Oceanogr. Lett., 5, 384-392, 10.1002/lol2.10161, 2020.

Wang, B., Liao, Q., Fillingham, J. H., and Bootsma, H. A.: On the coefficients of small eddy and surface divergence models for the air-water gas transfer velocity, J. Geophys. Res.-Oceans, 120, 2129-2146, 10.1002/2014JC010253, 2015.

Zappa, C. J., McGillis, W. R., Raymond, P. A., Edson, J. B., Hintsa, E. J., Zemmelink, H. J., Dacey, J. W. H., and Ho, D. T.: Environmental turbulent mixing controls on air-water gas exchange in marine and aquatic systems, Geophys. Res. Lett., 34, L10601, 10.1029/2006GL028790, 2007.